

Dear the Editor,

Thank you for your and reviewer's suggestion. The details of revision are listed below.

For example, line 8 and 39: there is an extra space here. Please remove and check the rest of the text.

**Reply:** Done.

line 40: 'mirco' should be 'micro'

**Reply:** Done.

line 137: 'In about 500 ml diluted ammonia.'

**Reply:** Done.

line 217: remove one of the dots.

**Reply:** Done.

line 243 and elsewhere: should be 'C. leptoporus' rather than 'Ca. leptoporus'.

**Reply:** Done. We also change the 'Cy. floridanus' to 'C. floridanus' and 'Co. pelagicus' to 'C. pelagicus'

line 234: perhaps add Tremblin et al. 2016 - PNAS in the papers using the micro filtering technique.

Answer: The method of Tremblin's research was same as Minoletti et al., which has been cited in the Introduction part.

Regarding equation 2-2: could you take a step towards isolating the effects of particle size, particle shape, particle material density, vessel shape, suspension density... etc? I don't see this as essential to the present manuscript, if the intention is purely to improve the protocol.

**Reply:** We think the equation 2-2 is for describing the method, so perhaps it's better to keep it simple. We had shown the equation special for the shape, particle density and suspension in other equations in the 'Discussions' part and made a summary in the 'Suggestions' part.

Line 150: This currently reads as though the vessel is smaller than the particle, and thus doesn't make sense.

"A significant wall effect will be detected when a particle is settling in a vessel which diameter is smaller than the particle size by two orders of magnitude (Barnea and Mizarchi, 1973)"

**Reply:** Yes, we realized this is an ambiguous sentence. We changed it as "...when a particle is settling in a vessel with a diameter that is smaller than **100 times of the particle size**". Thank you for pointing it out.

Regarding comment 9 by reviewer #2: although a Monte Carlo approach is indeed common, it is a rather opaque method of estimating uncertainty when the exact inputs are not specified. The uncertainty in a value is quite as important as it's expected value so it is therefore important to be clear about what goes into this analysis. The author's explanation here may be acceptable, but this does not mean that details of their approach should be omitted. A description of the above should at least go into the appendix for anyone who wants to reproduce their results.

**Reply:** We think we have offer enough information for reproducing the error estimation. Because the Poisson distribution is different from the normal distribution: the exception is equal to the variance. That means we don't have to describe the specified inputs such as the variance, which is a quite important parameter for other methods. We listed the name of matlab functions in the new version in the line 573-574 to make it easier to reproduce the results.

Regarding comment 14 by reviewer #2: the ratio: " $Nu(t=0) / D$ " is the number of coccoliths per unit thickness.  $dD$  doesn't come into it as you're not taking a derivative with respect to  $D$ . Please adjust.

**Reply:** We had replaced the ' $dD$ ' by unit thickness, so there is no ' $dD$ ' in the current version.

The description in appendix D is much improved. The assumptions have been stated more clearly than in the first version. One point however is that when equation D-1 is presented, it should be made clear that either A) as written this is for a coccolith of a single size, with all coccoliths sinking at

identical rates. Or B) that the variables  $N_u$  and  $v$  are actually distributions. It is not obvious a priori how these distributions will change throughout the course of settling and thus whether it's valid to use the mean of the distribution for all calculations.

**Reply:** We added the assumption: the velocity is the average sinking velocity. This assumption will be proved in the following (line 504-506).

It is appreciated that the authors due diligence showing that constant velocity throughout settling is reasonable. This is useful and should at least be stated explicitly as a reasonable assumption.

**Reply:** We added this reason of this assumption in the line 506-508 without any detail calculations.

# 1 A refinement of coccolith separation methods: Measuring the sinking

## 2 characters of coccoliths

3 Hongrui Zhang<sup>1,2</sup>, Heather Stoll<sup>2</sup>, Clara Bolton<sup>3</sup>, Xiaobo Jin<sup>1</sup>, Chuanlian Liu<sup>1</sup>

4 <sup>1</sup> State Key Laboratory of Marine Geology, Tongji University, Shanghai, 200092, China

5 <sup>2</sup> Geological Institute, Department of Earth Science, Sonneggstrasse 5, ETH, 8092, Zürich, Switzerland

6 <sup>3</sup> Aix-Marseille Univ, CNRS, IRD, Coll de France, CEREGE, Aix en Provence, France.

7 *Correspondence to:* Chuanlian Liu ([liucl@tongji.edu.cn](mailto:liucl@tongji.edu.cn))

8 **Abstract.** Quantification sinking velocities of individual coccoliths will contribute to optimizing  
9 laboratory methods for separating coccoliths of different sizes and species for geochemical analysis.  
10 The repeat settling/decanting method was the earliest method proposed to separate coccoliths from  
11 sediments, and is still widely used. However, in the absence of estimates of settling velocity for non-  
12 spherical coccoliths, previous implementations have depended mainly on time consuming empirical  
13 method development by trial and error. In this study, the sinking velocities of coccoliths belonging  
14 to different species were carefully measured in a series of settling experiments for the first time.  
15 Settling velocities of modern coccoliths range from 0.154 to 10.67 cm h<sup>-1</sup>. We found that a quadratic  
16 relationship between coccolith length and sinking velocity fits well and coccolith sinking velocity  
17 can be estimated by measuring the coccolith length and using the length-velocity factor,  $k_v$ . We  
18 found a negligible difference in sinking velocities measured in different vessels. However, an  
19 appropriate choice of vessel must be made to avoid 'hindered settling' in coccolith separations. The  
20 experimental data and theoretical calculations presented here support and improve the repeat  
21 settling/decanting method.

## 22 1. Introduction

23 Coccolithophores are some of the most important phytoplankton in the ocean. They can secrete  
24 calcareous plates called coccoliths, which contribute significantly to discrete particulate inorganic  
25 carbon in the euphotic zone and to CaCO<sub>3</sub> fluxes to the deep ocean (e.g., Young and Ziveri, 2000;  
26 Sprengel et al., 2002). Coccolith morphology, geochemistry and fossil assemblage composition  
27 can reflect paleoenvironmental changes (e.g., Beaufort et al., 1997; Stoll et al., 2002; Zhang et al.,  
28 2016). However, the use of coccolith geochemical analyses in paleoenvironmental reconstructions  
29 was so far hindered by the difficulty of isolating coccolith compared with foraminifera. Two main  
30 methods have been developed to concentrate near-monospecific assemblages of coccoliths from  
31 bulk sediments: one is the method based on a decanting technique (Paull and Thierstein, 1987; Stoll  
32 and Ziveri, 2002) and the other is that based on microfiltration (Minoletti et al., 2009). The  
33 improvement of separation techniques offered a new perspective to study the Earth's history (e.g.  
34 Stoll, 2005; Beltran et al., 2007; Bolton and Stoll, 2013; Rousselle et al., 2013). Moreover, the  
35 development of coccolith oxygen and carbon isotope studies in culture in recent years (e.g. Ziveri  
36 et al., 2003; Rickaby et al., 2010; Hermoso et al., 2016; McClelland et al., 2017) has provided an  
37 improved mechanistic understanding of coccolith isotope data and therefore stimulated the need for  
38 more purified coccolith fraction samples from the fossil record.

39 Both decanting and microfiltering are widely used methods for coccolith separation.— The  
40 microfiltering method separates coccoliths with polycarbonate ~~micro~~micro-filter membrane (with  
41 pore sizes of 2µm, 3µm, 5µm 8µm, 10µm and 12µm). This method is highly effective in the larger  
42 size ranges, but is very time consuming in sediments with a high proportion of small (<5µm)  
43 coccoliths (which tends to be the case in natural populations). It is also impossible to separate  
44 coccoliths with similar lengths by microfiltration, such as *Florisphaera profunda* and *Emiliana*  
45 *huxleyi* (Hermoso et al., 2015). Decanting, on the other hand, is highly effective for the small-sized  
46 coccoliths, because their slow settling times permit a greater ability to separate different sizes.  
47 Consequently, in some studies, a combination of the micro filtering and sinking or centrifugation  
48 method were applied for coccolith separation (Stoll, 2005; Bolton et al., 2012; Hermoso et al., 2015).  
49 The repeated sinking/decanting method, first employed by (Edwards, 1963; Paull and Thierstein,  
50 1987) follows the simple principle formalized by Stokes' Law for spherical particles: particles of

51 larger size settle more quickly because they have a higher ratio of volume and mass (accelerating  
52 sinking) to sectional area (resistance retarding sinking).— However, the sinking velocities of  
53 coccoliths with complex shape are difficult to calculate and have not been quantified in previous  
54 studies. Consequently, the repeated decanting method has generally used settling times based on  
55 empirical trial and error.

56 In the current study, we present a novel and rigorous estimation of –sinking velocity for 16 species  
57 of modern and Cenozoic coccoliths, carefully measured in 0.2% ammonia at 20°C. With this new  
58 dataset, we explore how to estimate the sinking velocity of coccoliths based on their shape and  
59 length, which allows our estimations to be generalized for other species, and for situations where  
60 the mean length of coccoliths of a given species was different from that of our study. –These  
61 generalizations, together with our results on sinking velocities of one coccolith species  
62 (*Gephyrocapsa oceanica*) in different vessels, should allow a significant improvement in efficiency  
63 of future protocols for separation of coccoliths by repeated decanting.

## 64 **2. Materials and methods**

### 65 **2.1 Sample selections**

66 We measured the sinking velocity of 16 different species of coccoliths, isolated from eight deep-sea  
67 sediment samples from the Pacific and Atlantic Oceans (Figure 1, Table A1). Sample were  
68 principally of Quaternary age but include two Neogene/Paleogene samples. In general, numbers of  
69 small coccoliths, including *E. huxleyi*, *Gephyrocapsa* spp and *Reticulofenestra* spp. are about an  
70 order of magnitude greater than that of larger coccoliths. However, the larger coccoliths'  
71 contributions to carbonate can be as high as 50% (Baumann, 2004; Jin et al., 2016). Moreover, both  
72 small coccoliths and large coccoliths are useful in geochemical analyses (Ziveri et al., 2003; Rickaby  
73 et al., 2010; Candelier et al., 2013; Bolton et al., 2012, 2016; Bolton and Stoll, 2013). Therefore,  
74 both small and large coccoliths were studied in this research. (B). Pictures of the studied coccolith  
75 are shown in Appendix B, and all classifications follow Nannotax3 except *Reticulofenestra* spp.  
76 (Figure C2 in Appendix C).

77 **2.2 Experiment designs**

78 **2.2.1 Sample pretreatments**

79 The sinking velocity measurement depends on absolute abundance estimation (more details in 2.2.2).  
80 However, on microscope slides, larger coccoliths and foraminifer fragments may cover smaller  
81 coccoliths, reducing the accuracy of coccolith absolute numbers. Thus, before sinking experiments  
82 were carried out, raw sediments were pretreated to purify the target coccoliths to reduce errors in  
83 coccolith counting. The raw sediments were disaggregated in 0.2% ammonia and sieved through a  
84 63 µm sieve and then treated by sinking method or filtering method (Bolton et al., 2012; Minoletti  
85 et al., 2009) to concentrate the target species up to at least more than 50% of the total assemblage  
86 (for Noëlaerhabdaceae coccoliths, a percentage more than 90% can be easily achieved). In one  
87 sample with aggregation (ODP 807), we did a rapid settling (30 min, 2 cm) to eliminate aggregates.  
88 Most of the species were measured individually in settling experiments, except for *Pseudoemiliana*  
89 *lacunosa* and *Umbilicosphaera sibogae*, which were measured together.

90 **2.2.2 Measuring the sinking speeds of coccoliths**

91 We are not aware of any prior direct determination of the sinking velocity of individual coccoliths,  
92 although the sinking velocities of live coccolithophores and other marine algal cells have been  
93 successfully measured by the 'FlowCAM' method (Bach et al., 2012) or a similar photography  
94 technique (e.g. Miklasz and Denny, 2010). Here we introduce a simple method to measure the  
95 particle sinking speeds without special equipment.

- 96 1. After pretreatment, the coccolith suspensions were gently shaken and then moved into  
97 comparison tubes which were vertically mounted on tube shelves. We set the timer going  
98 and let the suspension settle for a specified period of time, marked as sinking time or  
99 settling duration (T);
- 100 2. Thereafter, we removed the upper 15 ml supernatant into a 50 ml centrifuge tube with a 10  
101 ml pipette. This operation was performed slowly and gently to avoid drawing lower  
102 suspensions upward. The absolute counting of coccolith was achieved by using the 'drop  
103 technique' to make quantitative microscope slides (Koch and Young, 2007; Bordiga et al.,  
104 2015). 0.3 ml mixed suspension was extracted and pipettes onto a glass cover and dry the  
105 slider on a hotplate;

- 106 3. The lower suspension was than to homogenized and another slider was prepare as described  
 107 above;
- 108 4. The number of coccoliths in the upper and lower suspensions were carefully counted on  
 109 microscope at  $\times 1250$  magnification and the number of coccoliths and fields of view (FOV)  
 110 were recorded for further calculations. More than 300 specimens were counted for most of  
 111 the measurements. For the *Helicosphaera carteri* measurements, more than 100 FOV were  
 112 checked and about 100 specimens were counted.

113 To calculate the sinking velocities of coccoliths, we define a parameter named the separation ratio  
 114 (R), which represents the percentage of removed coccoliths in one separation by pumping out the  
 115 upper suspension. This parameter is important and will be repeatedly mentioned in the following  
 116 part. R was measured using the following equation (more details about derivation can be found in  
 117 Appendix D):

$$118 \quad R = \frac{\frac{N_1}{n_1} \times V_1}{\frac{N_1}{n_1} \times V_1 + \frac{N_2}{n_2} \times V_2} \quad (2-1)$$

119 where  $N_1$  and  $N_2$  are numbers of coccoliths counted in upper and lower suspension slides,  
 120 respectively;  $n_1$  and  $n_2$  are the number of FOV counted.  $V_1$  and  $V_2$  are the volume of the settling  
 121 vessel defined by the settling distance, as shown in Figure 2.

122 The separation ratio, R, also has a relationship with sinking time, T (Appendix D):

$$123 \quad R = \frac{V_1 - \frac{V_1}{D} \times v \times T}{V_1 + V_2} \quad (2-2)$$

124 where  $V_1$ ,  $V_2$  and D are shape parameters shown in Figure 2; and v is the average sinking velocity  
 125 of measured coccoliths. If we plot R against T, the slope of line has a relationship with v. Then liner  
 126 regressions between R and T were processed with MATLAB to calculate the v (details about error  
 127 analyses can be found in Appendix E).

128 There are still two issues to be explained. Firstly, - to eliminate the shape differences among vessels,  
 129 all separation ratios have been transferred to calibrated separation ratios ( $R_{cal}$ ), which means the  
 130 separation ratio measured in a standard vessel with  $V_1=15$  ml,  $V_2=10$  ml and  $D=6$  cm (more details  
 131 about transformation from R to  $R_{cal}$  can be found in Appendix D). Secondly, we treated the average  
 132 sinking velocities as the sinking velocities of the coccoliths with the average length. This  
 133 approximation has been proved reasonable in Appendix D.

134 **2.2.3 Detecting the potential influence of vessels**

135 Seven commonly used vessels were selected to detect the potential influence of vessels (Figure 3).  
136 Two of them are made of plastics (No.2 and No.3 in Figure 3) and all others are pyrex glass vessels.  
137 About 500 mg of sediment from core KX21-2 were pretreated as described in 2.2.1 and suspended  
138 in about 500 ml diluted ammonia. After that, settling experiments were performed as described in  
139 2.2.2 using different vessels. In these experiments, only the dominant species, *G. oceanica*, was  
140 measured.

141 **2.2.4 Other factors influencing the sinking velocity**

142 Temperature can change the density and viscosity of liquid. Generally speaking, the higher the  
143 temperature is, the lower the density and viscosity will become and the faster pellets will sink. Take  
144 water for instance, if the temperature increases from 15 to 30°C, the particle sinking velocity will  
145 increase by ~43% (Table 1). All sinking velocities measured or discussed in the following sections  
146 were velocities at 20°C to minimize the influence of temperature.

147 The calibration of sinking velocity in high concentration suspension has been calculated by  
148 Richardson and Zaki (1954)

149 
$$v = v_0(1 - \alpha_s)^{2.7} \quad (2-3)$$

150 where the  $\alpha_s$  is the solids volume fraction. Based on equation 2-3, the higher the suspension  
151 concentration is, the slower the sinking velocity will be. That is so called 'hindered settling'. When  
152 the  $\alpha_s=0.2\%$ , the reduction of sinking velocity owing to hindered settling is negligible ( $v/v_0$  equals  
153 99.46%). Hence, in this study all suspensions have solid volume fractions lower than 0.2% to avoid  
154 notable reductions of coccolith sinking velocities.

155 **3. Results and Discussions**

156 **3.1 Influence of vessels**

157 The sinking velocities of *G. oceanica* in the core KX21-2 in 0.2% ammonia at 20°C measured in  
158 different vessels vary from 0.99 to 1.23 cm h<sup>-1</sup>. The lowest value occurred in the 100 ml centrifuge  
159 tube and the highest sinking velocity was measured in the 50 ml centrifuge tube experiments. The  
160 correlations between sinking velocities and different vessel parameters are quite low:  $r=0.13$  for the  
161 vessel inner diameter,  $r=0.0005$  for the sinking distance and  $r=0.051$  for the upper volume and total



162 volume ratio ( $V_1/(V_1+V_2)$ ). The dissipation of energy by friction between the moving fluid and the  
163 walls can cause a reduction of sinking speed (wall effect). A significant wall effect will be detected  
164 when a particle is settling in a vessel with a diameter that is smaller than ~~the 100 times of the~~ particle  
165 size ~~by two orders of magnitude~~ (Barnea and Mizarchi, 1973). The length of coccoliths is on the  
166 micron scales, so the diameters of vessel used in laboratory are more than four orders of magnitude  
167 larger than coccoliths. Moreover, our results show that the difference between vessel materials, glass  
168 and plastics, can also be ignored (Figure 4). Hence, we suggest that vessel type almost has no  
169 significant influence on sinking velocity of coccoliths.

170 However, our experiments were premised on the basis that the concentration of suspension was  
171 equal among different vessels. This means that large vessels can treat more sediment at one time but  
172 if we choose a larger vessel, more suspensions should be pumped and it often costs more time in  
173 sinking (often due to longer sinking distance). Assuming that the sediment is composed of 50%  
174 calcite (with density of  $2.7 \text{ g cm}^{-3}$ ) and 50% clay (about  $1.7 \text{ g cm}^{-3}$ ), the largest amount of sediment  
175 that can be used without significant reduction of the sinking velocity (5%) is about 400 mg in 100  
176 ml suspension (this calculation is based on equation 2-3). However, because sediments accumulate  
177 in the lower suspension, the particle concentration can be more than 4 times higher than in the initial  
178 homogenous concentration. This phenomenon will be more significant for a vessel with a narrow  
179 bottom, such as centrifuge tubes. To avoid this, we recommend using about 100 mg dry sediment  
180 suspended in at least 100 ml suspension to avoid 'hindered settling'. If more sediment is necessary  
181 for geochemistry analyses, then a larger vessel should be selected to separate enough sample at one  
182 time.

### 183 **3.2 Sinking velocities at 20°C in 0.2% ammonia**

184 We measured the separation ratios of different coccoliths in comparison tubes at 20°C in 0.2%  
185 ammonia (Figure 5). The sinking velocities of coccoliths were then calculated by linear fitting of  
186 separation ratios and settling durations. The sinking velocities of studied coccoliths vary by two  
187 orders of magnitude from  $0.154 \text{ cm h}^{-1}$  to  $10.67 \text{ cm h}^{-1}$  (Table 2). The highest sinking velocity was  
188 found in the measurement of *Coccolithus pelagicus* and the lowest velocity was found for *F.*  
189 *profunda*. The average sinking speed of coccoliths is about 10-50% of the terminal sinking velocities  
190 of calcite spheres calculated by Stokes' Law (Figure 6c). These ratios are comparable to the oval

191 objects (e.g. seeds) data from Xie and Zhang (2001) and smaller than steel ellipsoids data from  
192 McNown and Malaika (1950). The sinking velocities of coccoliths measured in our experiment are  
193 about 2-3 orders of magnitude smaller than values from sediment traps of 143-243 m d<sup>-1</sup> (595~1012  
194 cm h<sup>-1</sup>) in the North Atlantic (Ziveri et al., 2000 and Stoll et al., 2007), suggesting that the coccoliths  
195 sinking out of the euphotic layer are mainly in the form of sinking aggregates rather than individual  
196 coccoliths.

### 197 3.3 Estimating the sinking velocities

198 Generally speaking, the sinking velocities of coccoliths increase with distal shield length (Figure  
199 5a), as expected from the increase in volume to sectional area for a given geometry as length  
200 increases. Our data implies that the sinking velocity has a power function relationship with distal  
201 shield length.

202 We propose that the sinking velocity of coccoliths might have a quadratic relationship with distal  
203 shield length as described by Stokes' Law (Figure 6a). If we use data for all species except *H. carteri*  
204 (the reason can be found in the following discussion), the sinking velocities can be described by the  
205 following equation:

$$206 \quad v = 0.0982 (\pm 0.001) * \phi^2 \quad (3-1)$$

207 Based on this quadratic regression, we derive a shape-velocity factor ( $k_v$ ) that relates settling  
208 velocity to coccolith length.

$$209 \quad v = k_v * \phi^2 \quad (3-2)$$

210 Furthermore, this factor is analogous to the shape-mass factor, ' $k_s$ ' used to relate coccolith mass to  
211 coccolith length (Young and Ziveri, 2000). The length and shape-velocity factor of coccoliths can  
212 be used to predict most of the sinking velocity variations, however, variations may also arise due to  
213 changes in coccolith mass and thickness, for a given length, and due to the hydrodynamics of  
214 particular shapes. We noticed that the smaller coccolith *G. caribbeanica* has a greater sinking  
215 velocity than the larger coccolith, *G. oceanica*. We suggest that this was caused by greater mass per  
216 length (or greater average thickness) in the case of *G. caribbeanica* and this may be due to the closed  
217 central area while *G. oceanica* has an open central area. Another example is *H. carteri*, which lower  
218 sinking velocity of which can be explained by the unique structure of *H. carteri* coccolith. Firstly,  
219 the broad edge of *H. carteri* can increase the drag force significantly. Moreover, most of the

220 measured coccoliths have a ellipticity (major axis length and minor axis length ratio) larger than 0.8,  
221 while the ellipticity of *H. carteri* is around 0.6, which means the mass of *H. carteri* is smaller than  
222 other species of coccoliths with similar lengths (Figure 6d and Figure C3). That is also the reason  
223 *H. carteri* was excluded from the general regression in equation 3-1. In the case of partial dissolution,  
224 the well-preserved *Cyclicargolithus floridanus* may have higher mass than dissolved (or  
225 disarticulated) *Cy. floridanus*, and therefore a slightly higher shape-velocity factor.

#### 226 **4. Suggestions for coccolith velocity estimations and separations**

227 To improve coccolith separation by settling methods, we measured sinking velocities of different  
228 coccoliths by gravity. Sinking velocities in this study varied from 0.154 to 10.61 cm h<sup>-1</sup>, about 10%  
229 to 50% of those of calcite spheres with same diameter. The shape of different vessels had little  
230 impact on the sinking velocity. But we should consider the volume of vessels to avoid ‘hindered  
231 settling’. The sinking velocities are mainly controlled by the shape of coccolith, including the distal  
232 shield length, the size of central area, and the ellipticity of coccoliths. Besides the shape of coccoliths,  
233 temperature is also crucial to the coccolith separations because of the dependence of sinking  
234 velocities on temperature. Length-velocity factors were proposed to estimate coccoliths sinking  
235 velocities, so coccolith separation can be achieved by following steps:

- 236 1. Measure the length of coccoliths in your target assemblage under the microscope and  
237 regress the length distribution by the assumption of normal distribution (details are in  
238 Appendix C);
- 239 2. Estimate sinking velocities for each important species. For species which sinking speed  
240 has been directly measured, we can use the length-velocity factor directly ( $v=k_v * \phi^2$ ).  
241 For unmeasured species, we can choose the length-velocity factor of coccoliths with  
242 similar morphology in this study or use the general length-velocity formula  
243 ( $v=0.098(\pm 0.001)* \phi^2$ );
- 244 3. Calculate the separation time for main species. For example, in KX21-2 there are three  
245 main coccoliths, *F. prounda*, *G. oceanica* and *C. leptoporus* and we wish to separate  
246 *G. oceanica* out from the bulk sediment. Calculate each coccoliths’ sinking velocity  
247 distributions as described in Step 2 above. As shown in Figure 7, a sinking velocity  
248 intermediate between *F. profunda* (with a length  $2\sigma$  larger than average, marked as  $+2\sigma$ )

249 and *G. oceanica* (with a length  $2\sigma$  smaller than average, marked as  $-2\sigma$ ) optimal to  
250 separate them, would be  $0.6 \text{ cm h}^{-1}$ . Similarly, we can chose speed thresholds  $1.85 \text{ cm}$   
251  $\text{h}^{-1}$  to separate *G. oceanica* from *Ca. leptoporus*. If we settle in a 50 ml centrifuge tube  
252 with a sinking distance,  $D$ , equal to  $5.84 \text{ cm}$ , the sinking time for separating *F. profunda*  
253 should be  $T=5.84/0.6=9.73 \text{ h}$ . Similarly, we can calculate the time for separating *G.*  
254 *oceanica* by  $T=5.84/1.85=3.16 \text{ h}$ ;

255 4. Homogenize the sediment suspension and let coccoliths settling as the period  
256 calculated in Step 3. After that, pump out the upper part of suspension. In the upper  
257 part, we have exclusively the smaller of the main coccoliths. However, column will  
258 still contain some smaller ones. So this step (settling and pumping) should be repeated  
259 until the lower part no longer has significant contribution from the smaller coccoliths.  
260 This step has been well described in pervious studies and more details can be found in  
261 Stoll and Ziveri (2002) and Bolton et al. (2012).

262 We find, if we use the general formula, a closed central area coccolith will sink faster than prediction  
263 (for *G. caribbeanica* and small *Ca. leptoporus* will settle  $\sim 40\%$  faster) and coccoliths with greater  
264 ellipticity can settle much slower (for *H. carteri* will settle as  $30\%$  of the predicted sinking velocity  
265 for coccolith with similar length). Moreover, the sinking method cannot separate every species of  
266 coccoliths perfectly. As mentioned in Section 2.2.1, *P. lacunosa* and *U. sibogae* cannot easily be  
267 separated from each other because they have similar sinking velocities. Nevertheless, this study  
268 provides the first direct estimation of coccolith settling velocities, which should simplify  
269 implementation of future methods to separate coccoliths by settling time.

270

271 *Acknowledgements.* This study was supported by grants from the Chinese National Science  
272 Foundation (91428310, 91428309 and 41530964, to L.C.). We thank the Integrated Ocean Drilling  
273 Program (IODP) for providing the samples. The IODP is sponsored by the U.S. National Science  
274 Foundation and participating countries under management of the IODP Management International,  
275 Inc (IODP-MI).

276 **Table 1.** The influence of temperature on sinking velocity. Density data is from Kell (1975) and  
 277 viscosity data is from Joseph et al. (1978).

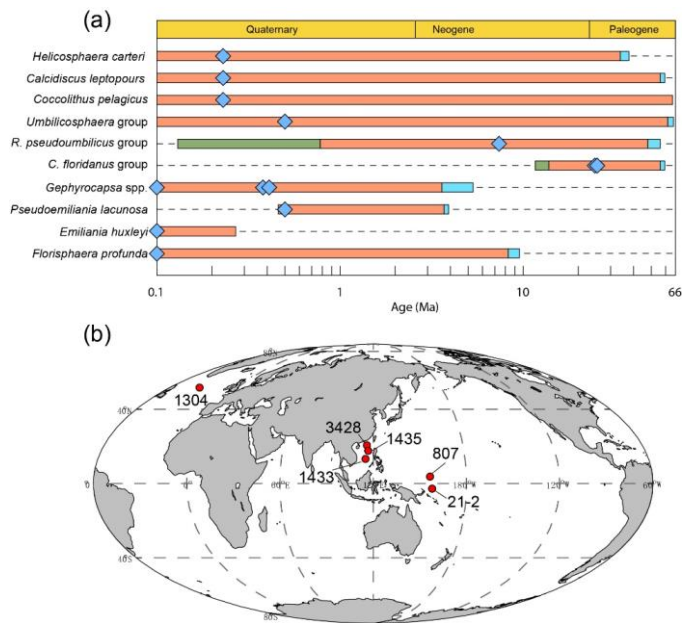
T (°C)	$\rho$ (g cm <sup>-3</sup> )	$\eta$ (mPa s)	$v_T : v_{T=20}$
15	0.9991	1.1447	0.8804
20	0.9982	1.0087	1
25	0.9970	0.8949	1.1279
30	0.9956	0.8000	1.2627

278 **Table 2.** The sinking velocity and shape-velocity factor of different coccolith species:  $\phi$  means the  
 279 distal shield length of coccolith and St  $\phi$  is the standard deviation of distal shield length; sv represents  
 280 the sinking velocity; v (95%-) and v (95%+) represent the lower and higher limit of 95% confidence  
 281 level, respectively. 'k<sub>v</sub>' represents the length-sinking velocity factor. The short name of coccolith can be  
 282 found in the caption of Figure 4. The details of coccoliths length distribution are in Appendix C.

Species	abb.	$\phi$ ( $\mu$ m)	St $\phi$ ( $\mu$ m)	sinking velocity (cm h <sup>-1</sup> )	v (95% -)	v (95% +)	k <sub>v</sub>
<i>F. profunda</i>	Fp-WP	1.508	0.557	0.158	0.010	0.011	0.070
<i>F. profunda</i>	Fp-SCS	1.786	0.641	0.154	0.051	0.052	0.048
small <i>Reticulofenestra</i>	Ret (<4um)	2.454	0.509	0.848	0.354	0.416	0.141
<i>E. huxleyi</i>	Emi	2.512	0.469	0.853	0.054	0.064	0.135
<i>Gephyocapsa</i> spp.	G spp	2.755	0.502	0.752	0.125	0.147	0.099
<i>G. caribbeanica</i>	Gear	3.312	0.352	1.873	0.174	0.192	0.171
<i>U. sibogae</i>	Umb	4.060	0.500	1.268	0.416	0.441	0.077
<i>G. oceanica</i>	Geo	4.187	0.517	1.170	0.155	0.178	0.067
<i>P. lacunosa</i>	Pla	4.350	0.617	1.171	0.337	0.338	0.062
Small <i>C<sub>2</sub>. leptoporus</i>	Cal small	4.605	0.629	3.351	0.172	0.199	0.158
large <i>Reticulofenestra</i>	Ret(>4um)	4.988	0.605	2.379	0.534	0.641	0.096
<i>C<sub>2</sub>. floridanus</i>	Cyf	5.805	0.963	4.174	0.320	0.336	0.124
(dissolved) <i>C<sub>2</sub>. floridanus</i>	Cyf -d	6.134	0.727	4.508	0.352	0.417	0.120
Large <i>C<sub>2</sub>. leptoporus</i>	Cal large	6.370	0.931	3.737	1.053	1.336	0.092
<i>H. carteri</i>	Hel	8.936	0.994	2.541	1.740	2.440	0.032
<i>Co. pelagicus</i>	Cpl	10.640	1.175	10.610	0.950	1.235	0.094

283

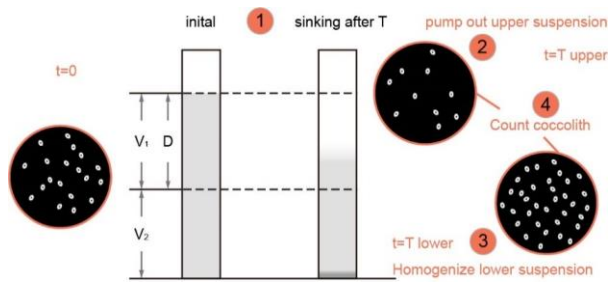
284 **Figure 1.** Temporal and spatial distribution of samples. (a) The evolution of studied coccoliths: first  
 285 occurrence and last occurrence data are from Nannotax3  
 286 (<http://www.mikrotax.org/Nannotax3/index.html>). The blue bars represent ranges of first occurrence  
 287 and the green bars represent ranges of last occurrence. The blue diamonds represent samples used in  
 288 this study. (b) Spatial distribution of samples. 1304 means IODP U1304, 3428 means MD12-3428cq,  
 289 1433 and 1435 means IODP U1433 and U1435, respectively. 807 means ODP 807 and 21-2 means  
 290 KX21-2.



291

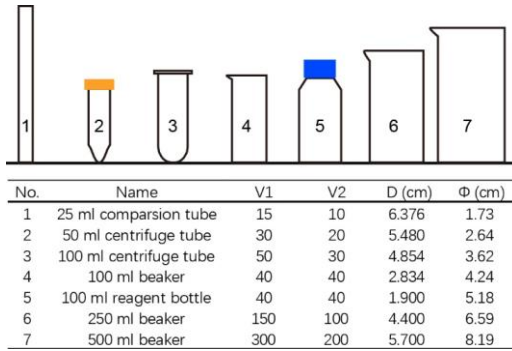
292

293 **Figure 2.** Schematic of settling experiments.  $V_1$  and  $V_2$  are the volumes of the upper and lower  
294 cylinders,  $D$  is the settled distance. The numbers in circles are same as the number of Steps described in  
295 Section 2.2.1.



296

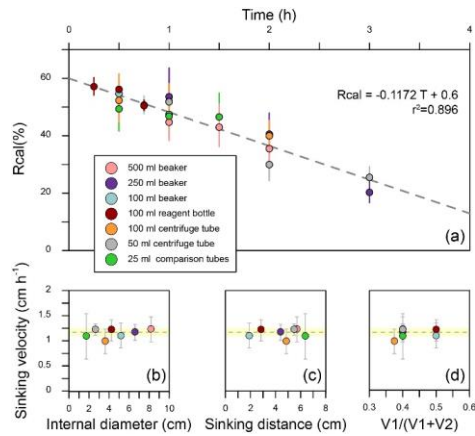
297 **Figure 3.** The shape parameters of vessels.  $V_1$  and  $V_2$  means the volume of upper suspension and lower  
 298 suspension, respectively.  $D$  means sinking distance.  $\Phi$  means average inner diameter which is  
 299 calculated by  $2 \cdot (V_1 / \pi D)^2$ .



300  
 301

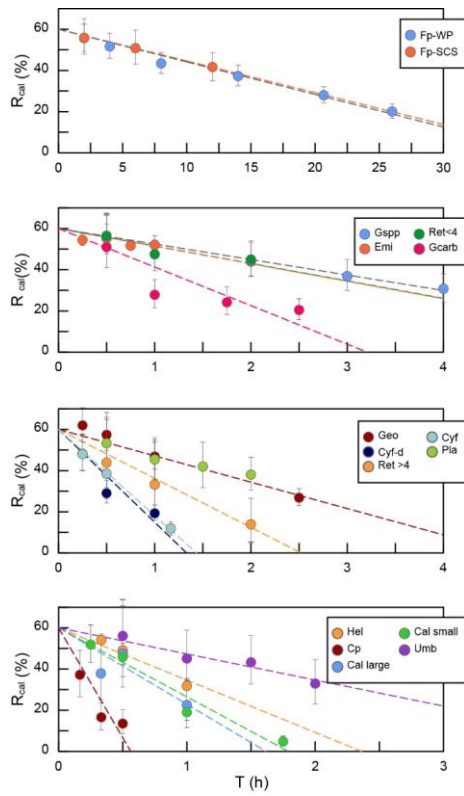


302 **Figure 4.** Sinking velocities of *G. oceanica* in the core KX-21-2 measured in different vessels. (a) The  
 303 calibrated separation ratios measured in different vessels. Error bars show 95% confidence level of  
 304 calibrated separation ratio. (b-d) The relationship between sinking velocity and different vessel shape  
 305 parameters. Error bars represent 95% confidence level of sinking velocity in each vessel and the shade  
 306 area represents 95% confidence level of sinking velocity considering all data points.



307

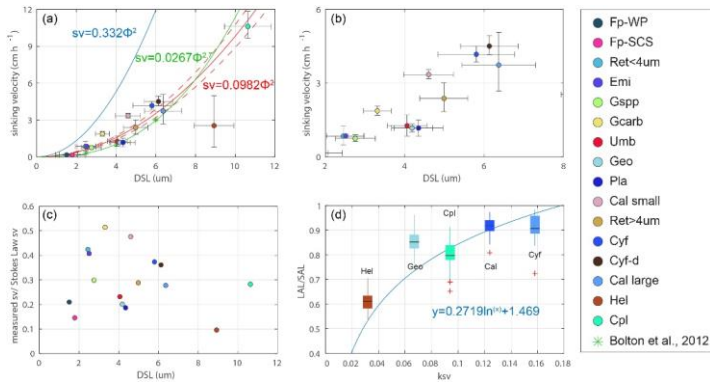
308 **Figure 5.** The calculated separation ratio (R<sub>cal</sub>) vs sinking duration. Fp-WP means *F. profunda* in the  
 309 West Pacific. Fp-SCS means *F. profunda* in the South China Sea. Emi means *E. huxleyi*. Gsp means  
 310 small *Geophycapsa*. Geo means *G. oceanica*. Gcarb means *G. caribbeanica*. Ret<4 means small  
 311 *Reticulofenestra*. Ret>4 means large *Reticulofenestra*. Cyf means *Cyclicargolithus floridanus*. Cy-d  
 312 means dissolved *Cy. floridanus*. Umb means *U. sibogae*. Pla means *Pseudoemiliana lacunosa*. Hel  
 313 means *H. carteri*. Cal large means larger *Calicidiscus leptoporus*. Cal small means small *Ca.*  
 314 *leptoporus*. Cpl means *Ca. pelagicus*.



315  
 316

317

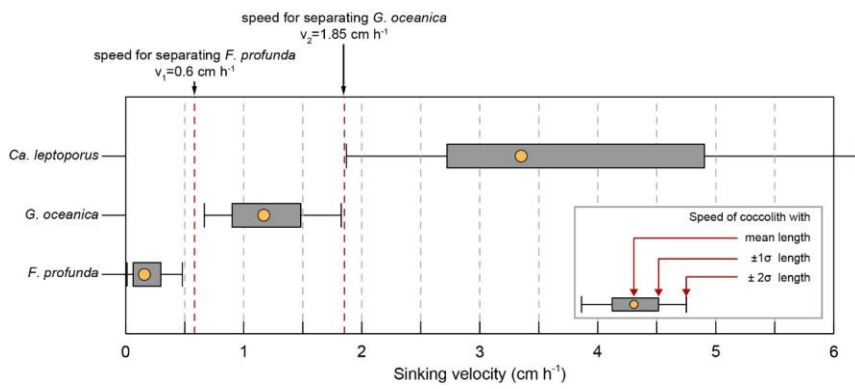
318 **Figure 6.** Coccolith sinking velocities and coccolith shape factors. (a-b) Sinking velocities and mean  
319 distal shield length. The horizontal error bars represent one standard deviation of coccolith length and  
320 the vertical ones represent 95% confidence level of measured sinking velocities. The blue, green and  
321 red lines represent sinking velocity of calcite sphere objects, coccolith sinking velocities estimated by  
322 Bolton et al. (2012) and this study, respectively. (c) The ratio of measured speed and speed calculated  
323 by Stokes' Law. (d) Coccolith short axis length (SAL) and long axis length (LAL) ratio against shape-  
324 velocity factor  $k_v$ . Box shows median value and upper/lower quartiles, whiskers show maximum and  
325 minimum values, outliers larger than 1.5 of the interquartile range are shown as red crosses. The SAL  
326 against LAL plot was shown in Figure C3. The short names of coccoliths can be found in Table 2.



327

328

329 **Figure 7.** The selection of separation velocities: the sinking velocities of three main coccolith species  
 330 in sample from core KX21-2 were calculated by the length distribution and velocity factors in Table 2.  
 331 The yellow dots represent sinking velocities of coccoliths with mean length. The edge of boxes show  
 332 the sinking velocities of coccolith within one standard deviation of length ( $\pm 1\sigma$ ) and the whiskers  
 333 mark the sinking velocities of coccolith within two standard deviation of length ( $\pm 2\sigma$ ).



334

335 **References**

- 336 Bach, L.T., Riebesell, U., Sett, S., Febiri, S., Rzepka, P., Schulz, K.G., 2012. An approach for  
337 particle sinking velocity measurements in the 3-400  $\mu\text{m}$  size range and considerations on  
338 the effect of temperature on sinking rates. *Mar Biol* 159, 1853-1864, doi:10.1007/s00227-  
339 012-1945-2.
- 340 Barnea, E., Mizrahi, J., 1973. A generalized approach to the fluid dynamics of particulate  
341 systems: Part 1. General correlation for fluidization and sedimentation in solid  
342 multiparticle systems. *The Chemical Engineering Journal* 5, 171-189, doi:10.1016/0300-  
343 9467(73)80008-5.
- 344 Baumann, K.-H., 2004. Importance of size measurements for coccolith carbonate flux estimates.  
345 *Micropaleontology*, 35-43.
- 346 Beaufort, L., Lancelot, Y., Camberlin, P., Cayre, O., Vincent, E., Bassinot, F., Labeyrie, L.,  
347 1997. Insolation cycles as a major control of equatorial Indian Ocean primary production.  
348 *Science* 278, 1451-1454, doi:10.1126/science.278.5342.1451.
- 349 Beltran, C., de Rafélis, M., Minoletti, F., Renard, M., Sicre, M.A., Ezat, U., 2007. Coccolith  
350  $\delta^{18}\text{O}$  and alkenone records in middle Pliocene orbitally controlled deposits: High-  
351 frequency temperature and salinity variations of sea surface water. *Geochemistry,*  
352 *Geophysics, Geosystems* 8, Q05003, doi:10.1029/2006GC001483.
- 353 Bolton, C.T., Hernandez-Sanchez, M.T., Fuertes, M.A., Gonzalez-Lemos, S., Abrevaya, L.,  
354 Mendez-Vicente, A., Flores, J.A., Probert, I., Giosan, L., Johnson, J., Stoll, H.M., 2016.  
355 Decrease in coccolithophore calcification and  $\text{CO}_2$  since the middle Miocene. *Nat*  
356 *Commun* 7, 10284, doi:10.1038/ncomms10284.
- 357 Bolton, C.T., Stoll, H.M., 2013. Late Miocene threshold response of marine algae to carbon  
358 dioxide limitation. *Nature* 500, 558-562, doi:10.1038/nature12448.
- 359 Bolton, C.T., Stoll, H.M., Mendez-Vicente, A., 2012. Vital effects in coccolith calcite:  
360 Cenozoic climate- $\text{pCO}_2$ drove the diversity of carbon acquisition strategies in  
361 coccolithophores, *Paleoceanography* 27, doi:10.1029/2012pa002339.
- 362 Bordiga, M., Bartol, M., Henderiks, J., 2015. Absolute nannofossil abundance estimates:  
363 Quantifying the pros and cons of different techniques. *Revue de micropaléontologie* 58,

364 155-165 doi:10.1016/j.revmic.2015.05.002.

365 Candelier, Y., Minoletti, F., Probert, I., Hermoso, M., 2013. Temperature dependence of  
366 oxygen isotope fractionation in coccolith calcite: A culture and core top calibration of the  
367 genus *Calcidiscus*. *Geochimica et Cosmochimica Acta* 100, 264-281,  
368 doi:10.1016/j.gca.2012.09.040.

369 Hermoso, M., Candelier, Y., Browning, T.J., Minoletti, F., 2015. Environmental control of the  
370 isotopic composition of subfossil coccolith calcite: Are laboratory culture data transferable  
371 to the natural environment? *GeoResJ* 7, 35-42, doi:10.1016/j.grj.2015.05.002.

372 Hermoso, M., Chan, I.Z.X., McClelland, H.L.O., Heureux, A.M.C., Rickaby, R.E.M., 2016.  
373 Vanishing coccolith vital effects with alleviated carbon limitation. *Biogeosciences* 13,  
374 301-312, doi:10.5194/bg-13-301-2016.

375 Jin, X., Liu, C., Poulton, A.J., Dai, M., Guo, X., 2016. Coccolithophore responses to  
376 environmental variability in the South China Sea: species composition and calcite content.  
377 *Biogeosciences* 13, 4843-4861, doi: 10.5194/bg-13-4843-2016.

378 Kell, G.S., 1975. Density, thermal expansivity, and compressibility of liquid water from 0. deg.  
379 to 150. deg.. correlations and tables for atmospheric pressure and saturation reviewed and  
380 expressed on 1968 temperature scale. *Journal of Chemical and Engineering Data* 20, 97-  
381 105.

382 Kestin, J., Sokolov, M., Wakeham, W.A., 1978. Viscosity of liquid water in the range -8 °C to  
383 150 °C. *Journal of Physical and Chemical Reference Data* 7, 941-948.

384 Koch, C., Young, J., 2007. A simple weighing and dilution technique for determining absolute  
385 abundances of coccoliths from sediment samples. *J. Nanoplankton Res.*

386 McClelland, H.L., Bruggeman, J., Hermoso, M., Rickaby, R.E., 2017. The origin of carbon  
387 isotope vital effects in coccolith calcite. *Nat Commun* 8, 14511,  
388 doi:10.1038/ncomms14511.

389 McClelland, H.L., Barbarin, N., Beaufort, L., Hermoso, M., Ferretti, P., Greaves, M., Rickaby,  
390 R.E.M., 2016. Calcification response of a key phytoplankton family to millennial-scale  
391 environmental change. *Scientific Reports* 6, 34263, doi: 10.1038/srep34263.

392 McNown, John S., and Jamil Malaika. "Effects of particle shape on settling velocity at low

393 Reynolds numbers." *Eos, Transactions American Geophysical Union* 31.1 (1950): 74-82.

394 Miklasz, K.A., Denny, M.W., 2010. Diatom sinkings speeds: Improved predictions and insight  
395 from a modified Stokes' law. *Limnology and Oceanography* 55, 2513-2525,  
396 doi:10.4319/lo.2010.55.6.2513.

397 Minoletti, F., Hermoso, M., Gressier, V., 2009. Separation of sedimentary micron-sized  
398 particles for palaeoceanography and calcareous nannoplankton biogeochemistry. *Nat.*  
399 *Protocols* 4, 14-24, doi:10.1038/nprot.2008.200.

400 Paull, C.K., Thierstein, H.R., 1987. Stable isotopic fractionation among particles in Quaternary  
401 coccolith-sized deep-sea sediments. *Paleoceanography* 2, 423-429,  
402 doi:10.1029/PA002i004p00423.

403 Edwards, A.R., 1963. A preparation technique for calcareous nannoplankton.  
404 *Micropaleontology* 9, 103-104.

405 Richardson, J., Zaki, W., 1954. The sedimentation of a suspension of uniform spheres under  
406 conditions of viscous flow. *Chemical Engineering Science* 3, 65-73.

407 Rickaby, R.E.M., Henderiks, J., Young, J.N., 2010. Perturbing phytoplankton: response and  
408 isotopic fractionation with changing carbonate chemistry in two coccolithophore species.  
409 *Clim. Past* 6, 771-785, doi:10.5194/cp-6-771-2010.

410 Rousselle, G., Beltran, C., Sicre, M.-A., Raffi, I., De Rafélis, M., 2013. Changes in sea-surface  
411 conditions in the Equatorial Pacific during the middle Miocene–Pliocene as inferred from  
412 coccolith geochemistry. *Earth and Planetary Science Letters* 361, 412-421,  
413 doi:10.1016/j.epsl.2012.11.003.

414 Sprengel, C., Baumann, K.-H., Henderiks, J., Henrich, R., Neuer, S., 2002. Modern  
415 coccolithophore and carbonate sedimentation along a productivity gradient in the Canary  
416 Islands region: seasonal export production and surface accumulation rates. *Deep Sea*  
417 *Research Part II: Topical Studies in Oceanography* 49, 3577-3598 doi: 10.1016/S0967-  
418 0645(02)00099-1.

419 Stoll, H.M., 2005. Limited range of interspecific vital effects in coccolith stable isotopic records  
420 during the Paleocene-Eocene thermal maximum. *Paleoceanography* 20,  
421 doi:10.1029/2004pa001046.

422 Stoll, H.M., Rosenthal, Y., Falkowski, P., 2002. Climate proxies from Sr/Ca of coccolith calcite:  
423 calibrations from continuous culture of *Emiliana huxleyi*. *Geochimica et Cosmochimica*  
424 *Acta* 66, 927-936, doi:10.1016/S0016-7037(01)00836-5.

425 Stoll, H.M., Ziveri, P., 2002. Separation of monospecific and restricted coccolith assemblages  
426 from sediments using differential settling velocity. *Marine Micropaleontology* 46, 209-  
427 221, doi: 10.1016/S0377-8398(02)00040-3.

428 Xie, H-Y., and D-W. Zhang. "Stokes shape factor and its application in the measurement of  
429 spherity of non-spherical particles." *Powder Technology* 114.1 (2001): 102-105 doi:  
430 10.1016/S0032-5910(00)00269-2.

431 Young, J.R., Ziveri, P., 2000. Calculation of coccolith volume and it use in calibration of  
432 carbonate flux estimates. *Deep sea research Part II: Topical studies in oceanography* 47,  
433 1679-1700, doi:10.1016/S0967-0645(00)00003-5.

434 Zhang, H., Liu, C., Jin, X., Shi, J., Zhao, S., Jian, Z., 2016. Dynamics of primary productivity  
435 in the northern South China Sea over the past 24,000 years. *Geochemistry, Geophysics,*  
436 *Geosystems* 17, 4878-4891, doi:10.1002/2016GC006602 .

437 Ziveri, P., Stoll, H., Probert, I., Klaas, C., Geisen, M., Ganssen, G., Young, J., 2003. Stable  
438 isotope 'vital effects' in coccolith calcite. *Earth and Planetary Science Letters* 210, 137-  
439 149, doi:10.1016/S0012-821X(03)00101-8.



440 **Appendix A. Sample selections**

441 **Table A1.** Sample selections

Measured coccolith	abb.	Region	Core	Section	Epoch	Age model ref.
<i>F. profunda</i>	Fp-SCS	SCS	MD12-3428	0-1 cm	Holocene	Zhang et al., 2016
<i>F. profunda</i>	Fp-WP	W.P.	KX21-2	2-4 cm	Holocene	Liang et al., 2016
<i>E. huxleyi</i>	Emi	SCS	MD12-3428	0-1 cm	Holocene	Zhang et al., 2016
<i>Gephyocapsa</i> spp.	Gspp	W.P.	ODP 807A	1H 5W 102-104	Pleistocene	Jin et al., 2010
<i>G. oceanica</i>	Geo	W.P.	KX21-2	2-4 cm	Holocene	Liang et al., 2016
<i>G. caribbeanica</i>	Gcarb	N.A.	IODP 1304B	7H 5W 69-70	Pleistocene	Channell et al., 2010
small <i>Reticulofenestra</i>	Ret<4	SCS	IODP 1433B	28R 2W 30-34	Miocene	Li et al., 2013
large <i>Reticulofenestra</i>	Ret>4	SCS	IODP 1433B	28R 2W 30-34	Miocene	Li et al., 2013
<i>Cyclicargolithus floridanus</i>	Cyf	SCS	IODP 1435A	6R 3W 25-29	Oligocene	Li et al., 2013
<i>Cyclicargolithus floridanus</i>	Cyf-d	SCS	IODP 1435A	8R 1W 27-31	Oligocene	Li et al., 2013
<i>Umbilicosphaera sibogae</i>	Umb	W.P.	ODP 807A	3H 5W 92-94	Pleistocene	Jin et al., 2010
<i>Pseudoemiliana lacunosa</i>	Pla	W.P.	ODP 807A	3H 5W 92-94	Pleistocene	Jin et al., 2010
<i>Helicosphaera carteri</i>	Hel	W.P.	ODP 807A	3H 5W 92-94	Pleistocene	Jin et al., 2010
large <i>Calcidiscus leptoporus</i>	Cal large	W.P.	ODP 807A	3H 5W 92-94	Pleistocene	Jin et al., 2010
small <i>Calcidiscus leptoporus</i>	Cal small	N.A.	IODP 1304B	7H 5W 69-70	Pleistocene	Channell et al., 2010
<i>Coccolithus pelagicus</i>	Cpl	N.A.	IODP 1304B	7H 5W 69-70	Pleistocene	Channell et al., 2010

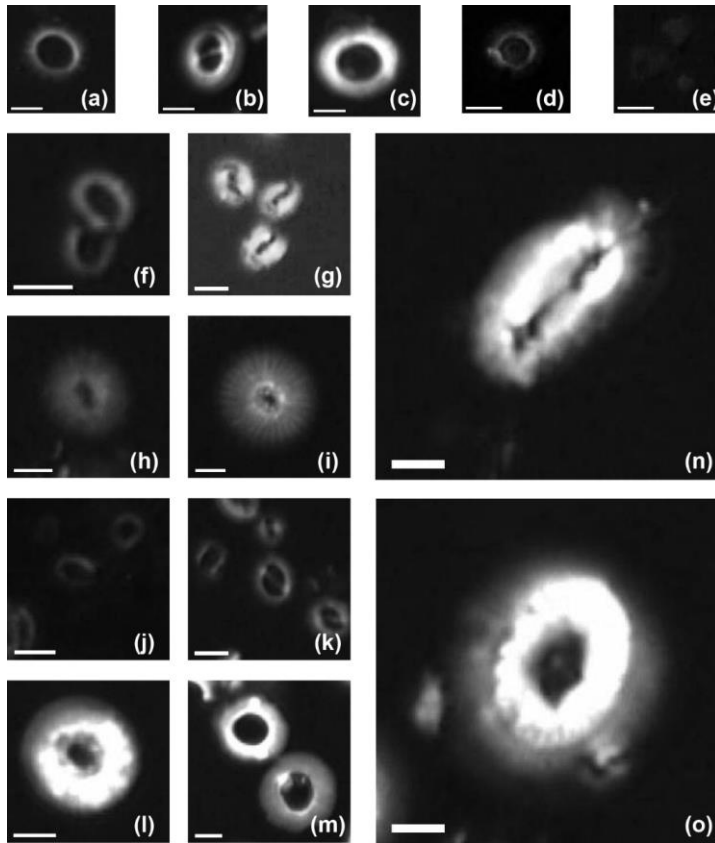
442

443 **References:**

- 444 Channell, J., Sato, T., Kanamatsu, T., Stein, R., Alvarez Zarikian, C., 2010. Expedition  
445 303/306 synthesis: North Atlantic climate. Channell, JET, Kanamatsu, T., Sato, T., Stein,  
446 R., Alvarez Zarikian, CA, Malone, MJ, and the Expedition 303, 306.  
447 Jin, H., Jian, Z., Cheng, X., Guo, J., 2011. Early Pleistocene formation of the asymmetric  
448 east-west pattern of upper water structure in the equatorial Pacific Ocean. Chinese  
449 Science Bulletin 56, 2251-2257.

- 450 Li, C.-F., Lin, J., Kulhanek, D.K., 2013. South China Sea tectonics: Opening of the South  
451 China Sea and its implications for southeastAsian tectonics, climates, and deep mantle  
452 processes since the late Mesozoic. IODP Sci. Prosp 349.
- 453 Liang, D., Liu, C., 2016. Variations and controlling factors of the coccolith weight in the  
454 Western Pacific Warm Pool over the last 200 ka. Journal of Ocean University of China  
455 15, 456-464.
- 456 Zhang, H., Liu, C., Jin, X., Shi, J., Zhao, S., Jian, Z., 2016. Dynamics of primary productivity  
457 in the northern South China Sea over the past 24,000 years. Geochemistry, Geophysics,  
458 Geosystems 17, 4878-4891.

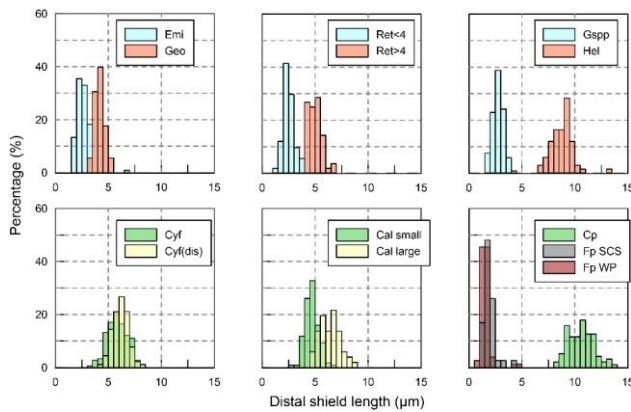
459 **Appendix B. Coccolith images under circular polarized light**



460  
 461 **Plate B1.** Imaged of measured coccolith in this study: (a) *Pseudoemiliana lacinosa* in the core ODP  
 462 807; (b) *Gephyrocapsa oceanica* in the core KX21-2; (c) *Reticulofenestra* spp. (large) in the core  
 463 IODP U1433B; (d) *Umbilicosphaera sibogae* in the core ODP 807; (e) *Florispharea profunda* in  
 464 the core KX21-2; (f) *Reticulofenestra* spp. (small) in the core IODP U1433B; (g) *Gephyrocapsa*  
 465 *caribbeanica* in the core IODP U1304B; (h) small *Calcidiscus leptoporus* in the core IODP U1304B;  
 466 (i) large *Calcidiscus leptoporus* in the core ODP 807A; (j) *Emiliana huxleyi* in the surface sediment  
 467 in the South China Sea; (k) *Gephyrocapsa* spp. in the core ODP 807; (l) *Cyclicargolithus floridanus*  
 468 in the core IODP U1435A and (m) dissolved *Cyclicargolithus floridanus* in the same core; (n)  
 469 *Helicosphaera carteri* in the core ODP 807A; (o) *Coccolithus pelagicus* in the core IODP U1304B.  
 470 White bars represent a length of 2  $\mu\text{m}$ .

471 **Appendix C. The length distribution of coccoliths**

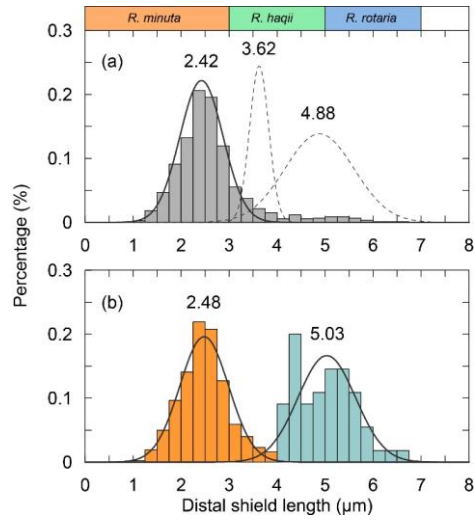
472 To measure the distal shield length of coccoliths, pictures were taken at a magnification of 1250x  
473 under circular polarized light. The coccolith lengths were measured by using the image analysis  
474 software, ImageJ. More than 5 pictures were taken and more than 50 (usually more than 100)  
475 coccolith specimens were measured. The length distributions of coccoliths measured in our  
476 experiments were shown in the Figure C1.



477

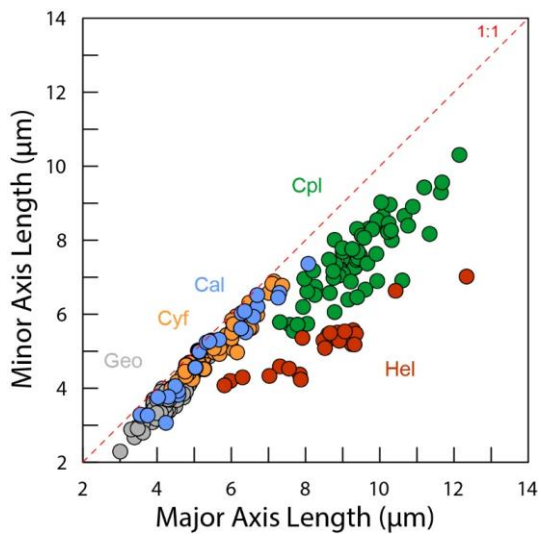
478 **Figure C1.** Size distribution of coccolith measured in the present study. The shorten names of coccolith  
479 follow Table A1.

480 The classification of coccoliths by length was supported by mixture analysis in PAST (Hammer et  
481 al., 2001), such as *Reticulofenestra* spp. and *Gephyrocapsa* spp. *Reticulofenestra* spp. in the  
482 Miocene were classified into two groups, Ret. (<4 µm) and Ret. (>4 µm). The traditional  
483 classification of *Reticulofenestra* spp. is <3 µm, 3-5 µm and 5-7 µm didn't pass the normal  
484 distribution test. Hence, in this study the *Reticulofenestra* spp. are divided at 4 µm (Figure C2).  
485 *Gephyrocapsa* spp. were classified by the shape of coccoliths into small *Gephyrocapsa* (central area  
486 opening and length <3.5 µm), *G. oceanica* (central area opening and length >3.5µm) and *G.*  
487 *caribbeanica* (closed central area) by the length and central area.



488

489 **Figure C2.** The classical classification of *Reticulofenestra* spp. (a) and the classification used in our  
 490 study (b). The curves represent the normal distribution fits of different coccolith groups and the dish  
 491 curve marks that the goodness of fit is below 0.2.



492

493 **Figure C3.** The short axis and long axis length distribution of coccoliths in Figure 6d.

494 **Reference.**

495 Hammer, Ø., Harper, D., Ryan, P., 2001. Paleontological Statistics Software: Package for  
496 Education and Data Analysis. *Palaeontologia Electronica*.

497 **Appendix D. Coccolith movement in gravity settling**

498 In this part, the derivation of equation will be explained in detail including proofs of several  
 499 assumptions mentioned in the methods part.

500 When the well mixed sediment begins to sink, the decrease of coccoliths number in the upper  
 501 suspension ( $N_u$ ) can be described as following equation:

502 
$$\frac{dN_u}{dT} = -\frac{N_{u(t=0)}}{D} \times v \quad (D-1)$$

503 where the D is the length of upper suspension and  $N_{u(t=0)} / D$  is the initial number of coccolith in  
 504 cross-section with a unit thickness, v is the mean sinking velocity of coccolith. In practice, the  
 505 velocities of coccoliths are different, so we assume the measured velocity is the mean sinking  
 506 velocity of bulk coccolith. This assumption will be proved valid in the following.- The particle can  
 507 reaches 99.9% of the maximum sinking velocity within only  $10^{-7}$  s, so we assume the particle sinks  
 508 as maximum velocity from the beginning of its settling.

Formatted: Superscript

509 Do integration for the equation D-1, we can get the variation of coccolith number in the upper  
 510 column over time:

511 
$$N_u = N_{u(t=0)} - \frac{N_{u(t=0)}}{D} \times v \times T \quad (D-2)$$

512 where T is settling time. After a period of time (T), we pump out the upper suspension. Here we  
 513 define the number of coccoliths in the upper supernatant dividing the total coccoliths number in the  
 514 tube ( $N_t$ ) as separation ratio (R), which represents the percentage of total coccoliths removed in one  
 515 separation. R can be expressed by

516 
$$R = \frac{N_u}{N_t} \quad (D-3)$$

517 Assuming all coccoliths are uniformly distributed in the suspension at the beginning of settling,  
 518  $N_{u(t=0)}$  has relationship with  $N_t$  as follow:

519 
$$\frac{N_{u(t=0)}}{N_t} = \frac{V_1}{V_1+V_2} \quad (D-4)$$

520 where  $V_1$  is the volume of upper suspensions and  $V_2$  is the volume of lower suspensions.

521 Combining the equation D-1, D-2, D-3 and D-4, we obtain the relationship between separation ratio,  
 522 R, and sinking velocity, v, as follow:

523 
$$R = \frac{N_u}{N_t} = \frac{N_{u(t=0)} - \frac{N_{u(t=0)}}{D} \times v \times T}{N_t} = \frac{V_1 - \frac{V_1}{D} \times v \times T}{V_1+V_2} \quad (D-5)$$

524 If we plot the R and T on a figure, the slope of the line is a function of  $V_1$ ,  $V_2$ , D and v. Since the

525  $V_1$ ,  $V_2$ ,  $D$  are known parameters, we say the slope of R-T is a function of  $v$ , which is exactly what  
526 we want.

527 Comparison tubes used in our experiments have the same  $V_1$  and  $V_2$  but different  $D$ . Other vessels  
528 used in other experiments have different  $V_1$ ,  $V_2$  and  $D$ . So we should adjust the raw separation ratio  
529 to calibrated separation ratio ( $R_{cal}$ ), which represents the separation ratio made in a standard vessel  
530 with  $V_{1std}=15$  ml,  $V_{2std}=10$  ml and  $D_{std}=6$  cm. This step can be described by equation D-6:

$$531 \quad R_{cal} = \frac{[R \times (V_1 + V_2) - V_1] \times D \times V_{1std}}{(D_{std} \times V_1 + V_{1std}) \times (V_{1std} + V_{2std})} \quad (D-6)$$

532 After calibrated, the slope of  $R_{cal}$ -T ( $k$ ) has relationship with  $v$  as following equation:

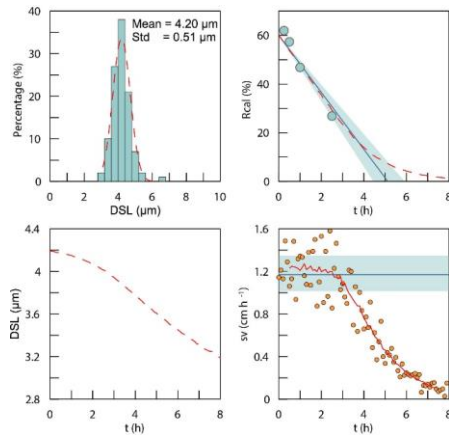
$$533 \quad v = -\frac{D_{std} \times (V_{1std} + V_{2std})}{V_{1std}} \times k = -10 \times k \quad (D-7)$$

534 where  $k$  is the slope of  $R_{cal}$  against T from regression and other parameters are as described above.

535 Hence, the sinking velocity of different coccoliths can be achieved by measuring the variations of  
536  $R_{cal}$  over time.

537 The coccoliths' lengths in the sediment have some variations. So what we measured is actually the  
538 bulk settling velocity of whole coccolith population. We also offer a test for the assumption that the  
539 average sinking velocity of all coccoliths can be treated as the sinking velocity of coccoliths with  
540 the average length. Here we used the data of *G. oceanica*. A normal distribution was fitted to the  
541 measured length distribution (Figure D1-a). We generated 100000 coccolith following the normal  
542 distribution and let these coccolith evenly distributing in the comparison tube at the initial and then  
543 set them sinking without collisions with each other. The sinking velocities of different size  
544 coccoliths were calculated by the velocity-shape parameter ' $k_v$ ' as described in discussion part. We  
545 modeled the coccoliths sinking process and computed the separation ratio (red dash line in Figure  
546 D1-b), coccolith length (red dash line in Figure D1-c) and instant sinking velocities (orange dots in  
547 Figure D1-d) at different time sections.





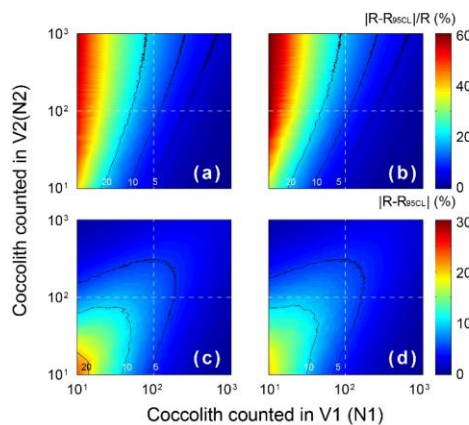
548  
549

550 **Figure D1.** The simulations of coccoliths settling with different lengths: (a) the length distribution of  
551 coccoliths. The green bars represent measured data and red dash line represents the best fit for normal  
552 distribution. (b) The calibrated separation ratio: the green dots are measured data in our settling  
553 experiments, the blue line and shade area represent the calculated sinking velocity based on  $R_{cal}$   
554 measurement and the red dash line represents results obtained from simulations. (c) The average length  
555 of removed coccolith in simulations; (d) the modeling sinking velocities of coccoliths: the orange dots  
556 are instant sinking velocity calculated from derivation of  $R_{cal}$ , the red dash line is weighted average for  
557 the instant sinking velocity. Blue line represents the average sinking velocity we measured and the  
558 green shade area represents 95% confidence level of the measured velocity.

559 For *G. oceanica* experiments, the instant sinking velocity would not change significantly until  
560 settling for more 3 hours. That means for all  $R_{cal}$  larger than 15% are safe for liner regressions. The  
561 minimum safe number of  $R_{cal}$  will descend with the drop of dispersion degree of coccolith length  
562 distribution. Hence our assumption for average sinking velocity and the use of liner regression are  
563 proved to be reasonable.

564 **Appendix E. Statistical and error analyses**

565 The errors of measured separation ratio (R) and calculated sinking velocity (v) are mainly caused  
566 by counting coccolith, the error of which follows the Poisson distribution. To detect the influence of  
567 counting number on the result error, the error of separation ratio was simulated by 5000 times Monte  
568 Carlo calculations with assumptions that ' $V_1:V_2=15:10$ ' and ' $n_1=n_2$ ' (Figure E1). The result shows  
569 that the number of coccolith counted in the upper column draws more influence on the relative error  
570 ( $|R-R_{95CL}|/R$ ). That means more coccolith in the upper suspension should be counted to make results  
571 more accurate. The slope of  $R_{cal-T}$  was calculated by liner fitting with the intercept fixed on  
572  $V_1/(V_1+V_2)$ . The input  $R_{cal}$  were generated from measured values considering the error of coccolith  
573 counting (by the Matlab function 'random'). The regressions of  $R_{cal-T}$  were repeated by 5000 times  
574 regressions in the software Matlab (by the function 'lsqcurvefit') and the error of sinking velocity,  
575 v, was source from the distribution slope of  $R_{cal-T}$  in Monte Carlo process.



576  
577 **Figure E1.** The error distribution with different  $N_1$  and  $N_2$  (ranging from 1 to 1000) simulated 5000  
578 times by the Matlab with assumptions that the error distributions of  $N_1$  and  $N_2$  follow Poisson  
579 distribution. The calculation of R follows equation 2-5, and here we assume numbers of FOV are equal  
580 ( $n_1=n_2$ ). Counter lines mark values equal to 5, 10 and 20. (a) and (c) represent the lower 95%  
581 confidence level and (b) and (d) represent upper 95% confidence level. (a) and (b) the relative error of  
582 R and (c) and (d) represent the absolute error of R.